Low-Frequency Waves and Traveling Storm Tracks. Part I: Barotropic Component

MING CAI AND HUUG M. VAN DEN DOOL

Cooperative Institute for Climate Studies, Department of Meteorology, University of Maryland, College Park, Maryland

(Manuscript received 25 September 1990, in final form 15 January 1991)

ABSTRACT

We have documented with the observed Northern Hemispheric 500 mb geopotential height data for ten winter seasons that traveling storm tracks exist downstream of the troughs of traveling low-frequency waves. The relation between the low-frequency flow and the traveling storm tracks is discovered with a novel observational technique that records high-frequency activity in a framework traveling along with an identifiable low-frequency structure. The vorticity flux of the high-frequency eddies associated with the traveling storm tracks acts both to reinforce the low-frequency waves and to retard their propagation.

These findings strongly indicate that a substantial amount of the low-frequency variability of the midlatitude atmospheric circulation is attributable to the forcing of the high-frequency eddies. These low-frequency waves organize the high-frequency eddies in such a way that the latter tend to intensify preferentially downstream of the troughs of the former. The symbiotic relation between the low-frequency flow and the traveling storm tracks is dynamically equivalent to the relation between the stationary waves and the stationary storm tracks. This mutual relationship is a necessary although not sufficient condition to parameterize high-frequency eddies in terms of low-frequency flow.

1. Introduction

The relation between the stationary waves and the synoptic scale eddies in the earth's atmosphere is a subject of continued interest. It is well known that the high-frequency eddies reach their highest amplitude preferentially downstream of the major troughs of the stationary waves, which statistically gives rise to the stationary storm tracks (Blackmon et al. 1977). The high-frequency transients organized by the stationary waves, on the other hand, tend to have a positive (negative) feedback effect upon the barotropic (baroclinic) component of the stationary waves (Lau and Holopainen 1984). The planetary scale waves, however, are rarely in their exact climatological positions. We therefore ought to address a complementary question about the relation between traveling planetary scale waves and the synoptic scale eddies. Our observational effort was very much motivated by a modeling study of Cai and Mak (1990b, hereafter referred to as CM) on the symbiotic relation between planetary and synoptic scale waves in an atmospheric model with zonally uniform forcing. It is found in CM that the internally generated traveling planetary scale wave is responsible for the existence of the model storm tracks that travel along with the planetary scale wave. The spatially coherent relation between the traveling planetary scale wave and its attendant storm tracks is dynamically reminiscent of the relation between the atmospheric stationary waves and the stationary storm tracks. In this study, we wish to determine observationally the role of the internal dynamics in generating the midlatitude atmospheric low-frequency waves and in organizing the synoptic scale eddies.

The forcing mechanism of the low-frequency variability by high-frequency eddies is one of the recurrent themes in the literature on the natural variability of the climate. It has been theoretically demonstrated that the nonlinear interactions alone may generate a substantial amount of low-frequency fluctuations in a zonally forced atmospheric model through a systematic energy transfer to the planetary scale waves from the baroclinically unstable synoptic scale waves (e.g., Gall et al. 1979; MacVean 1985; Hendon and Hartmann 1985). It also has been suggested in many observational and theoretical studies that the local forcing associated with the high-frequency eddies is a leading mechanism in maintaining a blocking flow (e.g., Green 1977; Shutts 1983; Hoskins et al. 1983; Illari 1984; Dole 1986; Mullen 1987; Holopainen and Fortelius 1987). The blocking flows, however, are rather exceptional (geographically fixed high amplitude cases), and it remains unclear whether the high-frequency forcing would be still working for the more common moderate and small amplitude low-frequency fluctuations. Moreover, most of the blocking case studies emphasized only the forcing by synoptic scale waves and not the reverse problem, namely, how such a blocking flow in turn organizes

Corresponding author address: Dr. Ming Cai, Department of Meteorology, University of Maryland at College Park, 2213 Computer & Space Science Bldg., College Park, MD 20742-2425.

the synoptic scale waves so that the later may continuously feed the former. Such interdependency between the high-frequency eddies and the low-frequency flow is a necessary although not sufficient condition to parameterize high-frequency eddies in terms of low-frequency flow. Metz (1987, 1990) has shown that the performance of a stochastically driven low-frequency model that is initially formulated by Egger and Schilling (1983, 1984) can be significantly improved if the "local relationship" between cyclone-scale and low-frequency eddies is taken into consideration.

Van den Dool (1982) and Kok et al. (1987) have shown that the forcing by synoptic scale eddies appears to be responsible for the major part of the monthly anomalies. Lau (1988) has identified the coupling relation between the monthly variability of the storm tracks and that of the stationary waves by diagnosing the dominant modes in the fluctuations of the second moment statistics of the high-frequency eddies. It was found that the eddy-induced geopotential tendency due to monthly fluctuations of the storm tracks accounts for a substantial amount of month-to-month variability of the stationary waves. Moreover, the modulation in the stationary waves takes place in such a way that the storm tracks are preferentially located downstream of the stationary troughs. Lau's study clearly indicates that such spatially coherent relation between the monthly variability of the storm tracks and that of the stationary waves closely resembles its counterpart in the climate mean.

This article is the first part of a study applying the theory and methodology proposed originally in CM to an atmospheric dataset to document statistically, on a day-to-day basis, the symbiotic relation between the low-frequency variability and the high-frequency eddies for a broad spectrum of low-frequency phenomena. The key questions to be addressed in this study are: "Are there traveling storm tracks that move along with traveling planetary scale waves? If so, what is the relation between the traveling storm tracks and the traveling planetary scale waves? What is the underlying physics that is responsible for such scale interaction and organization?" Answers to these questions would give us considerable insight about the origins of the low-frequency variability of the extratropic circulation and presumably may help to improve our forecast skill over times of weeks or longer.

The (stationary) storm tracks have mathematically been defined as the local maxima of the variance field associated with the high-frequency eddies. We here attempt to document if the general level (i.e., the zonally uniform part) of the variance field could arise from traveling storm tracks. From a practical point of view, the stationary storm tracks can be viewed as a manifestation of the existence of the geographically fixed asymmetric conditions at the bottom of the atmosphere, such as land–ocean contrast and large-scale topography. It has been demonstrated, however, in a number of theoretical studies that the formation of the stationary storm tracks is dynamically attributable to the local instability of a zonally inhomogeneous atmospheric time-mean flow[1] (e.g., Frederiksen 1983; Pierrehumbert 1984; Cai and Mak 1990a). It follows therefore that there should also exist traveling storm tracks associated with traveling planetary scale waves because there is no dynamic basis to distinguish the zonal inhomogeneity in the stationary planetary waves from that in the traveling planetary waves. Mullen (1987), Nakamura and Wallace (1990), and Mak (1990) indeed found an (instantaneous) storm track upstream of a (temporarily stationary) blocking circulation.

The focus of the first part of this study is on the existence of traveling storm tracks and the local forcing mechanism of such a traveling storm track upon the corresponding low-frequency flow using the 500 mb geopotential height field. According to CM's results, one should be able to deduce the synoptic forcing of the low-frequency fluctuations from one-level data since it mainly takes place in barotropic form. In the second part, we will attempt to determine the vertical structure of the low-frequency planetary scale waves and their associated traveling storm tracks with emphasis on organizing effects of the low-frequency flow on the high-frequency eddies.

Following CM, we shall employ a so-called phase shifting transformation to identify the time mean structure of a low-frequency planetary scale wave and its attendant traveling storm tracks. The phase shifting transformation essentially is a special composite analysis that follows the flow in a frame moving with a speed equal to the instantaneous phase speed of a planetary scale wave, so that the traveling planetary scale wave becomes stationary in the moving coordinate and so is its attendant storm tracks (if there are any).

Data used in this study is described in the next section. Section 3 contains a brief description of the wintertime climatology of the atmospheric statistics focusing on the relation between the stationary waves and the transients. This serves mostly as a reference for our study on the mutual dependence of the low-frequency flow and the high-frequency eddies. The phase shifting transformation used to identify the traveling storm tracks is introduced in section 4. Section 5 contains the results showing the traveling storm tracks associated with each of the first four low-frequency planetary scale waves and the forcing mechanism of

[1] Obviously, part of the zonal inhomogeneity in a time-mean flow may result from the geographically fixed asymmetric conditions at the bottom of the atmosphere. It should be emphasized, however, that part of the zonal inhomogeneity in a time-mean flow could also result from the forcing field induced by the associated stationary storm tracks themselves as suggested in the observational studies by Opsteegh and Vernekar (1982), Lau and Holopainen (1984) and the theoretical study by Cai and Mak (1990a).

the high-frequency eddies associated with the traveling storm tracks upon the low-frequency waves. The time-mean structure and propagation of the low-frequency planetary scale waves is also presented in this section. Section 6 is devoted to the issue of separation of traveling and stationary storm tracks with the means of the phase shifting method used in this study. Conclusions are given in section 7.

2. Data

The dataset used in this study are twice-daily 500 mb geopotential height derived from the U.S. National Meteorological Center (NMC) analyses for ten winters 1967/68 through 1976/77. The winter season is taken to be the 90-day period starting 1 December. The data are stored on a $4° \times 5°$ latitude–longitude grid covering the area from 22°N to the North Pole. Temporal data gaps (about 1.1%) were filled through a linear interpolation in time. The corrections were made by B. Doty and K. Mo and this dataset has been used in many observational studies (e.g., Van den Dool 1989).

A simple harmonic technique is used to separate the low-frequency fluctuations from the high-frequency eddies. Specifically, the data at each grid point in each winter season are temporally decomposed in the frequency domain ω_n, where $\omega_n = 2\pi n/90$ day^{-1}, $n = 1, 2, \cdots, 90$. The low-frequency and high-frequency components of the geopotential height are then obtained as

$$z^L(\lambda, \phi, t) = \sum_{n=1}^{14} [A_n(\lambda, \phi)\cos(\omega_n t) + B_n(\lambda, \phi)\sin(\omega_n t)],$$

$$z^H(\lambda, \phi, t) = \sum_{n=15}^{90} [A_n(\lambda, \phi)\cos(\omega_n t) + B_n(\lambda, \phi)\sin(\omega_n t)], \quad (1)$$

where, λ is longitude, ϕ is latitude, and t is time. Here A_n and B_n are the Fourier coefficients of the time series of the geopotential height at a grid point (λ, ϕ) in a winter season. Therefore, the time series z^L at each grid consists of the fluctuations with periods between a week and a season while z^H consists of the fluctuations with periods less than a week. The time-mean flow $\bar{z}(\lambda, \phi)$ of the ten winter seasons is determined as the average of the zero-frequency components of ten winters.

Of course, Eq. (1) is not a perfect filter since the time series is by no means periodic. A filtering technique such as employed by Blackmon (1976) has better characteristics in this regard. Also our (or any other) definition of high- and low-frequency fluctuations is somewhat arbitrary. But with broadband resolution sought, Eq. (1) should be adequate enough to distinguish the fluctuations in high and low frequencies. Indeed, the variance maps of the transients obtained with (1) have the same characteristics as those of others' studies in spite of the differences in the filtering technique and the definitions of the high- and low-frequency fluctuations (e.g., our Figs. 1b–c vs Figs. 3.1b–c in Wallace and Blackmon 1983).

The wave portion, $z^W(\lambda, \phi, t)$, of a flow $z(\lambda, \phi, t)$ can be obtained by performing a Fourier analysis in the zonal direction

$$z^W(\lambda, \phi, t) = \sum_{m=1}^{36} H_m(\phi, t)\cos\left(\frac{2\pi m\lambda}{360} + Q_m(\phi, t)\right), \quad (2)$$

where $H_m(\phi, t)$ and $Q_m(\phi, t)$ are the amplitude and the phase angle (in radians) of the wavenumber m at the latitude ϕ and time t, respectively.

3. Basic statistics

In this section, we present statistics of the stationary waves, the low-frequency fluctuations, and the stationary storm tracks of the ten winter seasons. The emphasis is on the relation between the stationary waves and the transients. It primarily serves to be a reference for the main theme of our study, namely, the symbiotic relation between low-frequency waves and traveling storm tracks.

Shown in Fig. 1a is the familiar time-mean flow of the ten winters. It is seen that there are two major troughs located along the east coasts of Asia and North America, associated with which are the two major jet streams. A third but much weaker trough is identifiable over central part of the Eurasian continent. The two zonally elongated local maxima over the exit regions of the climatological jet streams are the most notable features in the temporal root-mean-square (rms) field of the high-frequency eddies (Fig. 1b). They are commonly identified as the stationary storm tracks of the extratropic circulation. There is also a local maximum over the downstream region of the Eurasian trough. What has not been pointed out very often in the literature is the background value in the rms field of the high-frequency eddies, which may be measured by the minimum value of the rms field in the middle latitude band. According to Fig. 1b, the minimum value is about 40 gpm, which is still larger than the maxima in the high or low latitudes. We are used to identifying the climatological storm tracks as the local maxima of 70 or 80 gpm. But the background value is important here because part of it could arise from the traveling storm tracks. The rms field associated with the low-frequency fluctuations exhibits somewhat less zonally elongated maxima located farther downstream of the jet streams (Fig. 1c). They are the regions for the frequent occurrence of persistent, high-amplitude anomalies (Dole 1983). As documented in the earlier studies (e.g., Wallace and Blackmon 1983), the low-frequency

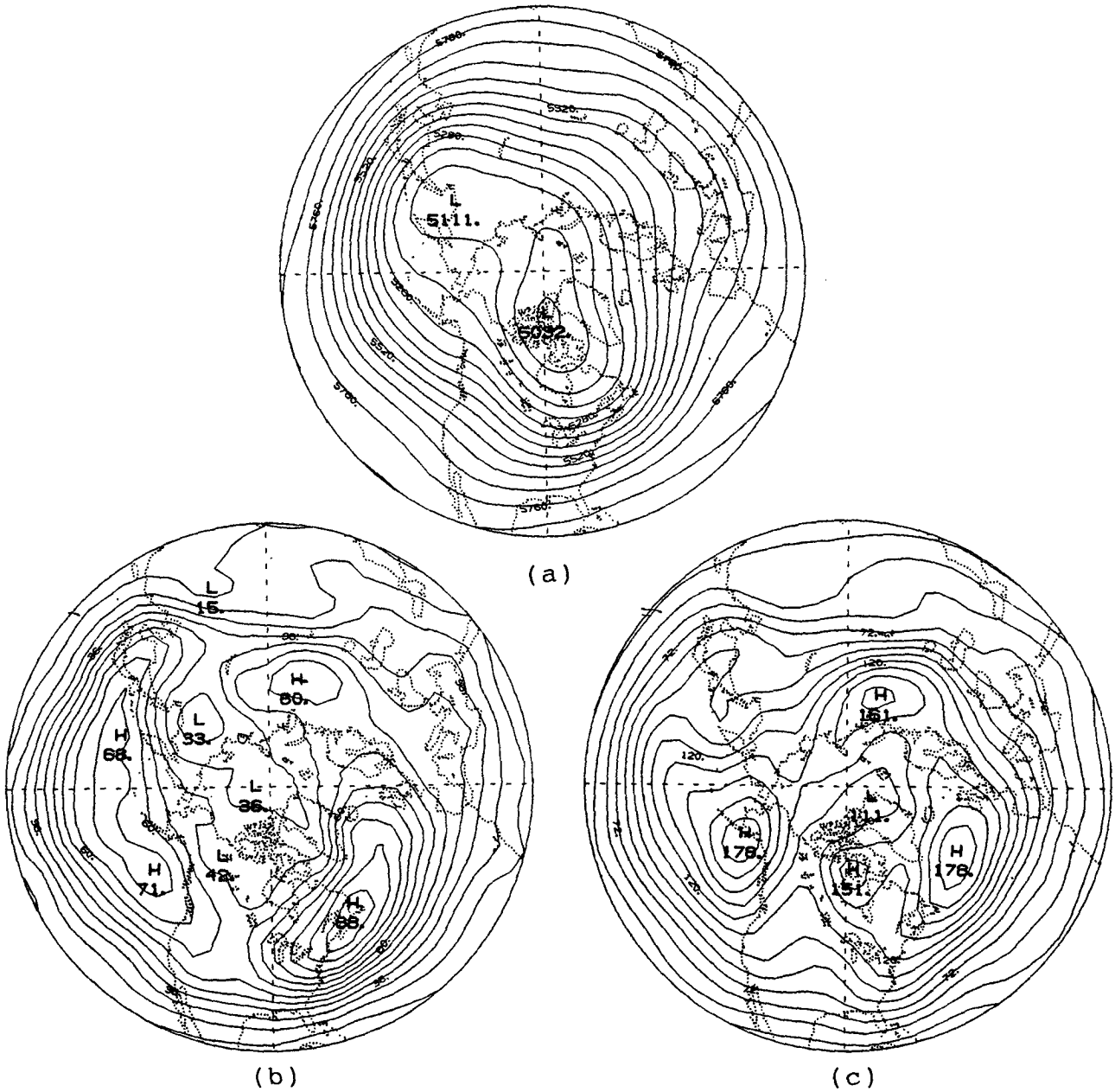

FIG. 1. Statistics of 500 mb geopotential height of the ten winter seasons. (a) Time-mean circulation. (b) Standard deviation of the high-frequency eddies. (c) Standard deviation of the low-frequency eddies. The contour intervals for panels (a), (b), and (c) are 60.0, 6.0, and 12.0 gpm, respectively.

variability in the height field is about twice as strong as the high-frequency variability.

Figure 2 displays a comparison of the time-mean amplitude of the stationary, low-frequency and high-frequency waves as a function of the zonal wavenumber at latitude 50°N. To our knowledge the statistics presented in Fig. 2 are not available in the literature (Blackmon 1976 showed that the power for frequency $1/15$ day^{-1} is maximum for planetary scale waves whereas that for frequency $1/5$ day^{-1} is maximum for synoptic scale waves). It is seen that wavenumber 1 is the dominant component in the stationary wave field and that the amplitude of the stationary waves drop abruptly as the zonal wavenumber increases beyond 3. The amplitude spectrum of the low-frequency waves is flat at the longer wave range ($m \leq 4$) and then decreases with increasing zonal wavenumber ($m \geq 5$) but the decrease is much slower than for the stationary waves. The amplitude spectrum of the high-frequency waves is relatively flat with a weak maximum at wave-

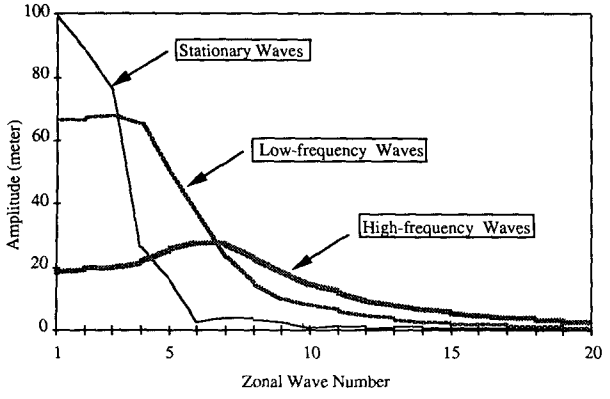

FIG. 2. The time-mean amplitude of the stationary, low-frequency, and high-frequency waves in 500 mb geopotential height at latitude 50° as a function of the zonal wavenumber.

number equal to 6 or 7. Figure 2 also suggests that the space and time scale of a disturbance are related. The calculations at other middle latitudes reveal the same result.

We have evaluated the instantaneous transient-eddy forcing field in terms of an eddy-induced geopotential tendency at each observation time for the ten winters according to

$$\chi(\lambda, \phi, t) \equiv \left(\frac{\partial Z}{\partial t}\right)^W = \nabla^{-2}\left(-\frac{f_0}{g} F^W\right)$$

$$= \nabla^{-2}\left\{-\frac{f_0}{g}[\nabla\cdot(\mathbf{v}'\zeta')]^w\right\}, \qquad (3)$$

where $\mathbf{v}'$ and ζ' are the geostrophic wind and vorticity determined from the transient part of the geopotential height z' [z' can be either $z^H(\lambda, \phi, t)$ or $z^L(\lambda, \phi, t)$], f_0 is the Coriolis parameter at 45° latitude, and g is the gravity constant. The superscript "w" in (3) stands for the wave portion of the corresponding field (i.e., zonal mean has been subtracted). Hence the χ field consists of only the wave portion of the feedback tendency field. The boundary condition for χ at 90°N is taken to be $\chi = 0$ since there is no wave at the pole. The boundary condition for χ at 22°N is artificially assumed to be $\partial\chi/\partial\phi = 0$. As found in Lau (1988), the solution for χ over most of the area poleward of 22°N is not sensitive to the particular treatment for the southern boundary condition except for the vicinity of the boundary. The time-mean of $\chi(\lambda, \phi, t)$ has been interpreted as the transient-induced forcing field upon the stationary waves (Lau and Holopainen 1984).

We solve (3) for χ with the boundary conditions proposed in the last paragraph by a relaxation method after replacing the spatial derivatives with centered finite difference formulas. Three other finite difference schemes (e.g., upstream, downstream, and semi-spectral) have been used as well. While the vorticity fluxes are somewhat sensitive to the numerical scheme, the results indicate little sensitivity in the χ field which is due to the smoothing effect of the inverse Laplacian operator.

Figure 3a plots the wave portion of the wintertime mean flow shown in Fig. 1a. We wish to compare it with the wintertime mean tendency fields induced by both high-frequency eddies and low-frequency fluctuations (Figs. 3b and 3c) and to illustrate the different roles of the transients in the two frequency bands in maintaining the stationary waves. In agreement with Lau and Holopainen (1984), the high-frequency eddies tend to reinforce the barotropic component of the stationary waves while the barotropic tendency field of the low-frequency eddies is nearly out of phase with the stationary waves. From an energetics point of view, the above statement is equivalent to stating that, on average, the high-frequency eddies (low-frequency flows) lose (gain) energy barotropically to (from) the stationary waves. This agrees with the findings of Simmons et al. (1983) and Branstator (1990) that the primary energy source for the low-frequency fluctuations is the conversion from the basic kinetic energy to disturbance kinetic energy. Cai and Mak (1990a) have shown that the cyclone-scale eddies excited through local baroclinic instability lose kinetic energy to the basic flow. The tendency field associated with the low-frequency eddies is twice as strong as that of the high-frequency eddies. This is primarily due to the fact that the low-frequency variability is twice as strong as the high-frequency variability (cf. Figs. 1b and 1c).

4. Method of phase shifting

As shown in Fig. 1b, the high-frequency transients tend to have larger amplitude over certain longitudinal sectors in middle latitudes than over others, indicating the existence of the stationary storm tracks. If, on the other hand, traveling storm tracks exist, they would only contribute to the zonally uniform part of the rms field and thus they would not show up in a preferred longitudinal sector. In order to detect traveling low-frequency waves and their associated traveling storm tracks, we have to travel along with the low-frequency waves. This enables us to construct the time-mean of the low-frequency flow and the rms map of the high-frequency transients in that moving frame. We shall refer to the flow "observed" in such a moving coordinate as the phase-shifted flow. Ideally, one should follow a specific trough (or ridge) of the total low-frequency flow to identify the (total) traveling storm tracks. Technically, this is not feasible because a trough (or ridge) usually disappears after some time. The alternative is to follow an identifiable structure of the low-frequency flow at a reference latitude, such as the ridge (or trough) of a particular low-frequency wave m_0 at the reference latitude. In order to make the detection of traveling storm tracks pure, all signals of the

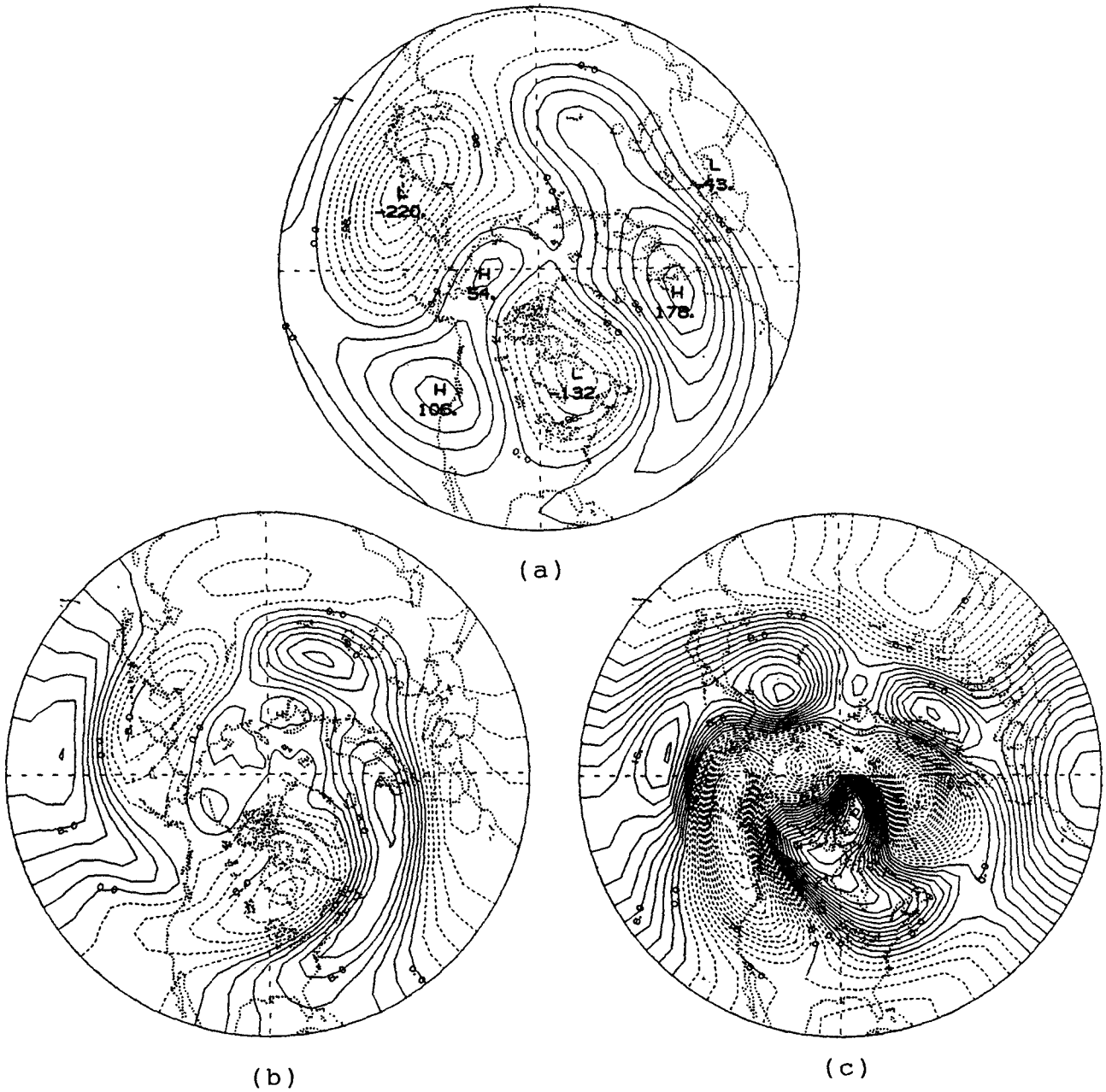

FIG. 3. (a) Total wave field of the time mean circulation shown in Fig. 1a. (b) Time-mean tendency field induced by the high-frequency eddies. (c) Time mean tendency field induced by the low-frequency eddies. The contour interval for (a) is 24.0 gpm and that for (b) and (c) is 2.0×10^{-5} gpm s^{-1}.

stationary storm tracks have to be removed. This is a major challenge addressed below at many places.

In general, we may construct a phase-shifted flow $\hat{z}(\lambda, \phi, t)$ at each time t from the original flow $z(\lambda, \phi, t)$ according to

$$\hat{z}(\lambda, \phi, t) = z(\lambda - \lambda^*(t; \phi_0), \phi, t), \qquad (4)$$

where, ϕ_0 is the reference latitude. It is obvious that the transformation (4) is no more than translating the whole flow at each time t eastward by an angle $\lambda^*(t; \phi_0)$. Therefore, the relative positions of troughs and ridges at each time are exactly preserved under this transformation. It follows that a manipulation with the phase-shifted flow can be accomplished by applying the phase-shift transformation to the fields resulting from the manipulation applied to the original flow, as long as the manipulation does not involve the time derivative. Particularly, a quantity derived from a

phase-shifted geopotential height $\hat{z}(\lambda, \phi, t)$, such as geostrophic wind and vorticity, is still meaningful and is exactly equal to its phase-shifted counterpart derived from the original flow $z(\lambda, \phi, t)$. The same is true for the product of two physical variables (e.g., vorticity fluxes).

The exact expression for $\lambda^*(t; \phi_0)$ is determined from a particular identifiable low-frequency structure. In this paper, we shall limit our discussions on the method of phase shifting following a particular low-frequency wave m_0 ($m_0 = 1, 2, 3$, and 4) at a reference latitude ϕ_0. In this case, the definition of $\lambda^*(t; \phi_0)$ is

$$\lambda^*(t; \phi_0) = \frac{360}{2\pi} \frac{Q^L_{m_0}(\phi_0, t) - Q^S_{m_0}(\phi_0) - 2\pi \mathcal{R}_{m_0}(t)}{m_0}, \tag{5}$$

where $Q^L_{m_0}(\phi_0, t)$ is the phase angle of the wave m_0 at latitude ϕ_0 of the low-frequency flow at time t. Here $Q^S_{m_0}(\phi_0)$ specifies the new longitude of the ridge of the wave m_0 at latitude ϕ_0 of the phase-shifted low-frequency flow.[2] The values of $\mathcal{R}_{m_0}(t)$ in (5) are $\mathcal{R}_1(t) \equiv 0$; $\mathcal{R}_2(t) = (0 \text{ or } 1)$; $\mathcal{R}_3(t) = (0, 1, \text{or } 2)$; $\mathcal{R}_4(t) = (0, 1, 2, \text{or } 3)$. The equiprobable values of $\mathcal{R}_{m_0}(t)$ are determined by a random number generator. The randomizer $\mathcal{R}_{m_0}(t)$ may be viewed as a purely mechanistic device, allowing us to select randomly the m_0 possible positions for the low-frequency wave m_0 with an equal possibility. Apart from the randomizer $\mathcal{R}_{m_0}(t)$, the phase shifting method (5) is the same as the one used in CM. We shall come back for the reason of introducing the randomizer $\mathcal{R}_{m_0}(t)$ in (5) in section 6.

The reference latitude ϕ_0 in (5) has to be in the middle latitudes since the zonally averaged rms of the high-frequency eddies as well as that of the low-frequency fluctuations reaches the maximum there. We have made a series of experiments with $42°\text{N} \leq \phi_0 \leq 62°\text{N}$. Most results are not very sensitive to the choice of the reference latitude ϕ_0 in this latitude band. Therefore, we shall in this article only report the results obtained with $\phi_0 = 50°\text{N}$.

5. Low-frequency planetary scale waves and the traveling storm tracks

This section reports the statistics of the 1800 phase-shifted flows relative to a low-frequency planetary scale wave with $m_0 = 1, 2, 3, 4$. The geographic locations of the statistics presented below are entirely determined by the choice of $Q^S_{m_0}(50°\text{N})$ in (5), which has been arbitrarily taken to be the phase angle of the corresponding stationary wave. Hence, only the relative geographical locations on these maps are dynamically meaningful, but not the absolute geographical longitudes.

a. Propagation of the low-frequency planetary scale waves

Shown in Fig. 4 are the normalized probability functions of $\Delta Q^L_{m_0}(t)$ for $m_0 = 1, 2, 3, 4$, where $\Delta Q^L_{m_0}(t)$ is defined as

$$\Delta Q^L_{m_0}(t) = -(Q^L_{m_0}(50°\text{N}, t) - Q^L_{m_0}(50°\text{N}, t - \Delta t)), \tag{6}$$

with Δt = one day. A positive (negative) $\Delta Q^L_{m_0}(t)$ means an eastward (a westward) propagation of the low-frequency wave m_0. The most striking feature in Fig. 4 is that the probability functions all have a narrowband distribution, indicating a gradual movement of the low-frequency waves. It is also seen for $m_0 = 1$, 2, 3 that the probability of a westward propagation is slightly larger than that of an eastward propagation. The low-frequency wave $m_0 = 4$ moves eastward more than it moves westward. We may estimate the time-mean phase speed of the wave m_0 from the time mean value of $\Delta Q^L_{m_0}(t)$ as

$$C_{m_0}(\phi_0) = \frac{\overline{\Delta Q^L_{m_0}(t)}}{m_0} \frac{a_0 \cos(\phi_0)}{\Delta t}, \tag{7}$$

where a_0 is the radius of the earth. It is found that $C_1(50°\text{N}) = -4.8 \text{ m s}^{-1}$; $C_2(50°\text{N}) = -1.8 \text{ m s}^{-1}$; $C_3(50°\text{N}) = -0.4 \text{ m s}^{-1}$; and $C_4(50°\text{N}) = 0.9 \text{ m s}^{-1}$.

We may also view $\Delta Q^L_{m_0}(t)$ defined in (6) as a measurement of the "smoothness" of the phase shifting transformation. A positive (negative) value of $\Delta Q^L_{m_0}(t)$ means that a relatively westward (eastward) phase shift has to be applied to the flow at time t. It is seen from Fig. 4 that at most times (>80%) we need to shift the flow by no more than $1/12$th of the wave length (or $\pm 30°$) of the reference wave per day.

b. Statistics of the phase-shifted flow with $m_0 = 1$

Shown in Fig. 5a is the time-mean circulation of the phase-shifted low-frequency flow with $m_0 = 1$. It primarily consists of the wavenumber 1 and therefore may be regarded as the time-mean structure of that traveling planetary scale wave. The dominance of $m_0 = 1$ could only be achieved by using several years of data. When we used only one winter season of data, $m_0 = 1$ showed up but mixed with several other waves. These mixed-in waves are different every year and disappear practically upon using all ten years of data.[3] The time-mean amplitude of the traveling wave $m_0 = 1$ is about 70%

[2] Arbitrarily but intentionally, we take $Q^s_{m_0}(\phi_0)$ to be the phase angle of the stationary wave m_0 at latitude ϕ_0. This allows easy comparison of the time-mean structure of the traveling planetary scale waves as well as the attendant rms statistics to the stationary counterparts.

[3] A similar statement is also applicable for the time mean circulations of the phase-shifted flows with $m_0 = 2$, 3, and 4 which will be presented in sections 5c–5e.

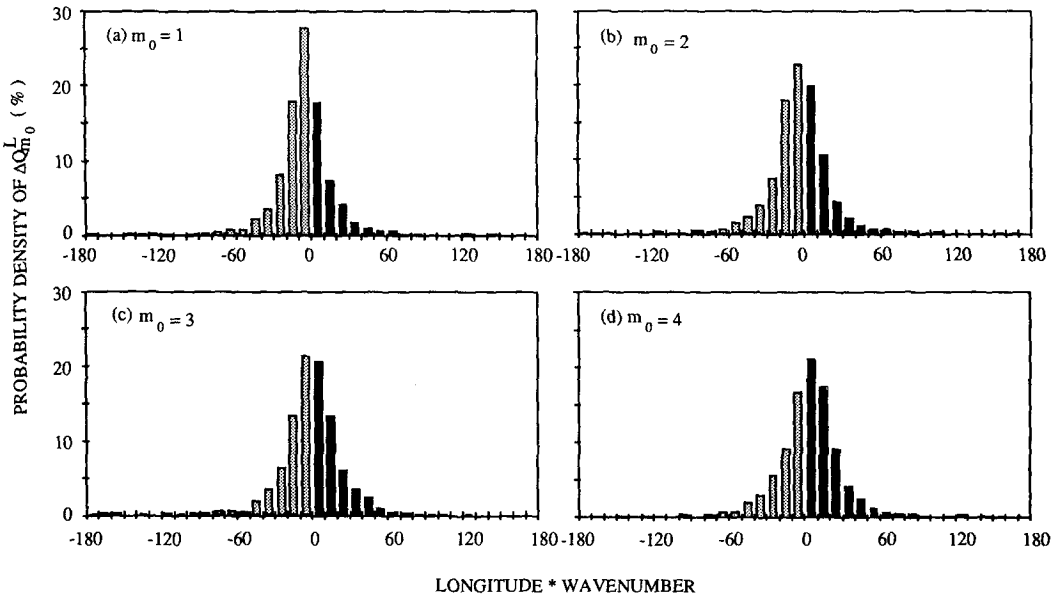

FIG. 4. Histograms of the phase change during a day of the traveling low-frequency waves. (a) $m_0 = 1$. (b) $m_0 = 2$. (c) $m_0 = 3$. (d) $m_0 = 4$.

of the amplitude of the stationary wavenumber 1 (cf. Fig. 2). In sharp contrast with the stationary wavenumber 1 (not shown here but see Fig. 9, Shabbar et al. 1990), the low-frequency wavenumber 1 changes its polarity from the tropics to the midlatitudes and from the midlatitudes to the higher latitudes. Madden and Speth (1989) also identified such meridional structure of the westward traveling wavenumber 1 in a composite study. This alteration of the polarity in the meridional direction of this low-frequency wave could be viewed as the manifestation of a dipolar (or tripolar) teleconnection pattern.

The rms of the high-frequency eddies phase-shifted relative to the low-frequency wave $m_0 = 1$ displays two storm tracks (Fig. 5b). The one on the left appears to be associated with the midlatitude trough shown in Fig. 5a. The central path of this storm track is about 45°N. The other one is linked to the high-latitude trough with the central path at about 55°N. Both storm tracks are embedded in a westerly anomaly flow, a recurrent feature. It is noted that the maxima of the rms shown in Fig. 5b are smaller than those shown in Fig. 1b. This, however, does not necessarily mean that the intensity of the traveling storm tracks is weaker than the stationary storm tracks. This is partly because what is shown in Fig. 5a are the traveling storm tracks associated with just one low-frequency planetary scale wave whereas the stationary storm tracks shown in Fig. 1b are associated with the total stationary waves.

Figure 5c is the map of the geopotential height tendency induced by the phase-shifted high-frequency eddies. The tendency flow also primarily consists of wavenumber 1. It also has the pattern of meridional alteration in the polarity. It is easy to see that the tendency field captures most of the main features shown in Fig. 5a, indicating a forcing mechanism of the low-frequency wave by its associated traveling storm tracks. The trough (or ridge) position of the tendency field over the midlatitude band appears to be a few degrees east of its counterpart shown in Fig. 5a. Recall that the low-frequency wave 1 travels westward in the mean. This implies that the vorticity flux by the high-frequency eddies on average tends to retard the westward propagation of the planetary scale wave.

c. Statistics of the phase-shifted flow with $m_0 = 2$

The time mean flow of the phase-shifted low-frequency flow with $m_0 = 2$ (Fig. 6a) is, as desired, characterized by wavenumber 2. This wave field has a dipolar pattern in the meridional direction, which again could account for some of the dipolar teleconnection patterns. Compared to its stationary counterpart, this traveling wave has smaller meridional scale. The rms of the phase-shifted high-frequency eddies relative to this low-frequency wave (Fig. 6b) reveals two major storm tracks downstream of the two troughs shown in Fig. 6a. The intensity of the traveling storm tracks is about the same as that associated with the traveling wavenumber 1. The downstream shift of the traveling storm tracks associated with the low-frequency wavenumber 2 is more pronounced than those for $m_0 = 1$ (Fig. 5). There are also two additional slightly weaker storm tracks over the northwest flank of the high pressure centers where the anomaly flow is westerly. The

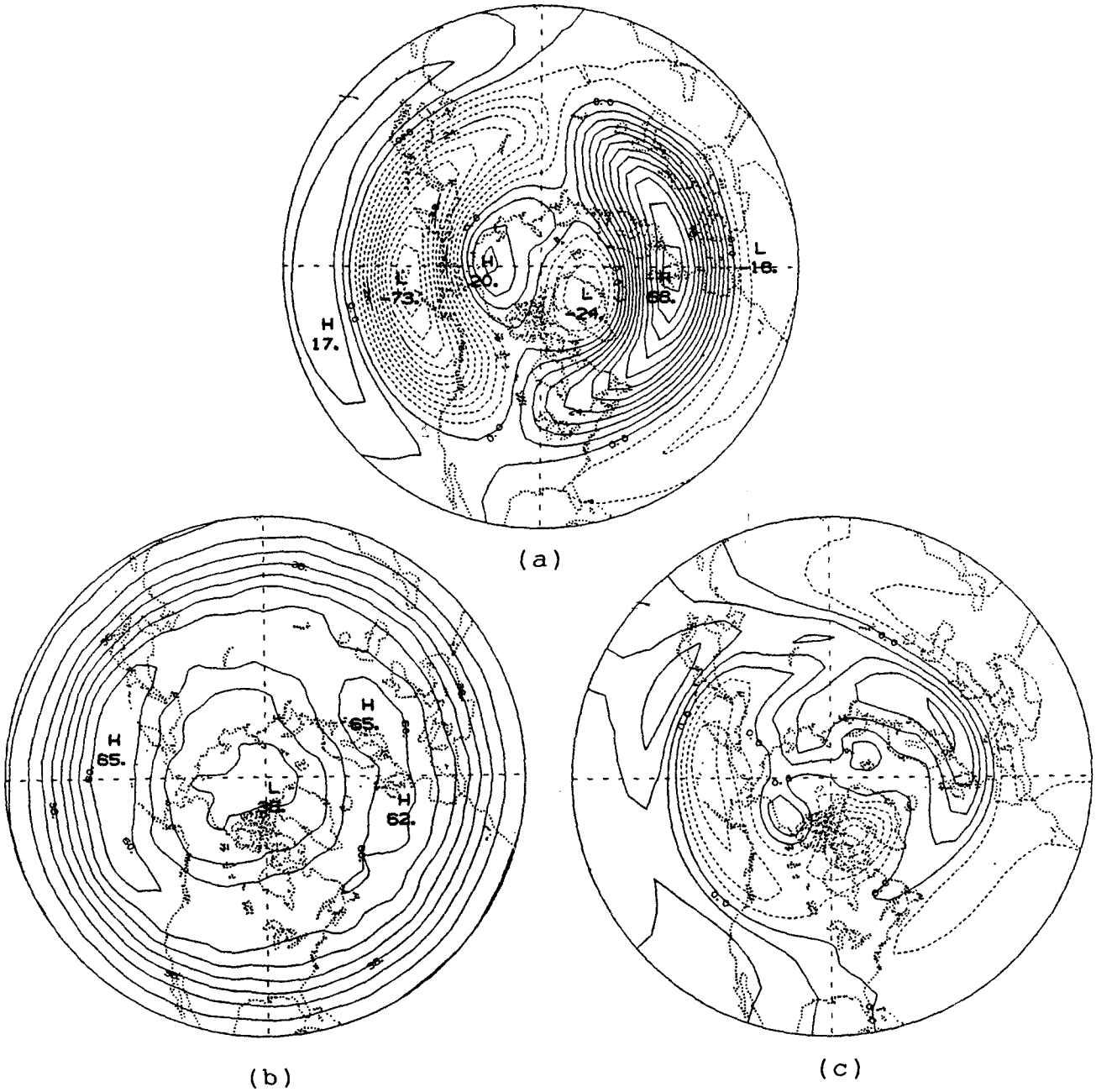

FIG. 5. Statistics of the phase-shifted flow with $m_0 = 1$. (a) Time-mean circulation. (b) Standard deviation of the phase-shifted high-frequency eddies. (c) Tendency-field induced by the phase-shifted high-frequency eddies. The contour interval for (a) and (b) is 6.0 gpm and that for (c) is 1.0×10^{-5} gpm s^{-1}. Only the relative geographical locations in this figure are dynamically meaningful but not the absolute geographical longitudes.

feedback field calculated with the phase-shifted high-frequency eddies (Fig. 6c) resembles closely the time-mean structure of the low-frequency wave. It is seen that the trough (or ridge) positions of the tendency field is slightly east of the low-frequency wave. Therefore, the vorticity flux associated with the high-frequency eddies tends to reinforce the low-frequency wavenumber 2 as well as to retard its westward propagation in the mean.

d. Statistics of the phase-shifted flow with $m_0 = 3$

The time-mean structure of the traveling planetary scale wavenumber 3 is shown in Fig. 7a. The amplitude of this wave is comparable to the stationary wavenum-

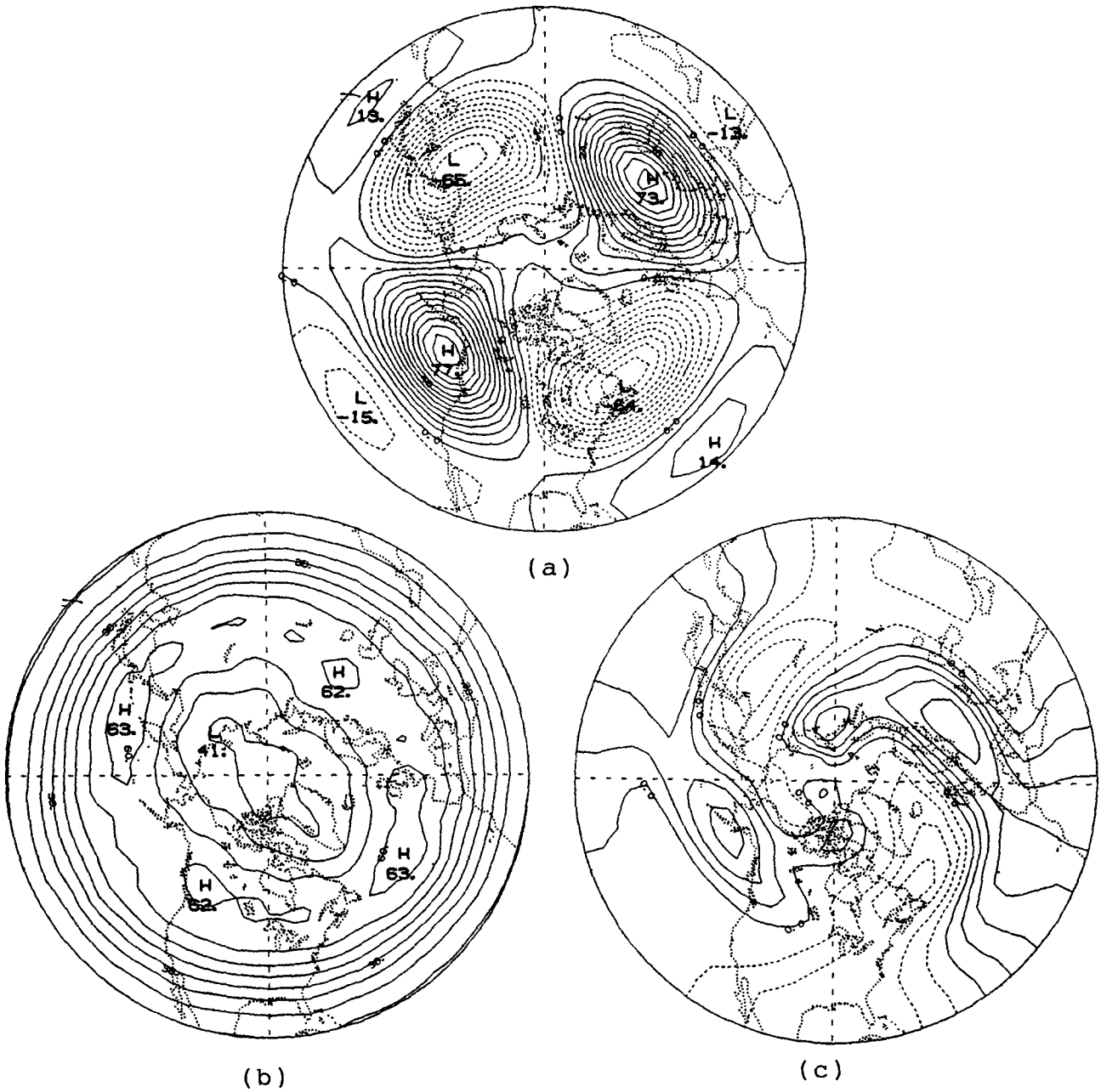

FIG. 6. As in Fig. 5 except for the phase-shifted flow with $m_0 = 2$.

ber 3. Like its stationary counterpart, its meridional structure is primarily monopole. The meridional scale of this low-frequency wave is about the same as its zonal scale. As shown in Fig. 7b, there is a well-defined storm track located at the downstream region of each trough of the traveling planetary scale wave. It is interesting to note that there are no storm tracks over the northern flank of the ridges in this case, in contrast to the cases of $m_0 = 1$ and 2. The feedback field of the corresponding phase-shifted high-frequency eddies mainly consists of the wavenumber 3 (Fig. 7c), indicating again the forcing mechanism of the planetary scale wave by its attendant storm tracks. The positions of the trough and the ridge of the feedback field now are to the west of their counterparts in the low-frequency flow. Therefore, the forcing field induced by the high-frequency eddies statistically tends to move low-frequency waves westward.

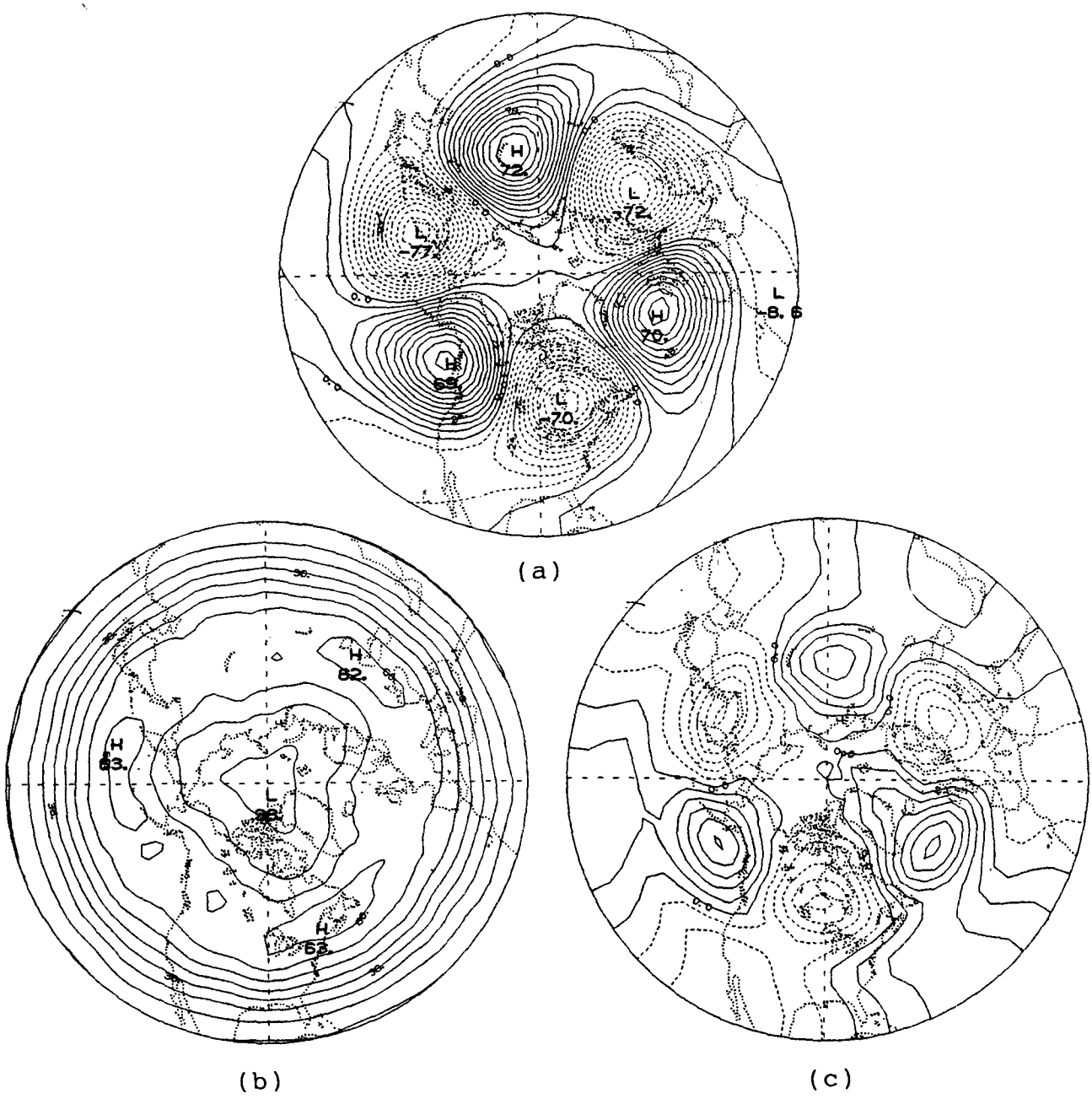

FIG. 7. As in Fig. 5 except for the phase-shifted flow with $m_0 = 3$.

e. Statistics of the phase-shifted flow with $m_0 = 4$

The time-mean flow of the phase-shifted low-frequency flow relative to the low-frequency wave $m_0 = 4$ (Fig. 8a) consists mainly of wavenumber 4. It has a monopole structure in the meridional direction. The amplitude of this wave is about twice as large as that of the stationary wavenumber 4 (cf. Fig. 2). There are four local maxima in the rms field of the corresponding phase-shifted high-frequency eddies (Fig. 8b). These maxima are located in downstream regions of the troughs of the traveling low-frequency wave. There is no evidence showing storm tracks associated with the ridges of this low-frequency wave. The tendency field induced by the four traveling storm tracks is dominated by wavenumber 4 (Fig. 8c). The lows and highs of the tendency field are slightly westward relative to the corresponding low-frequency wave. Therefore, the high-

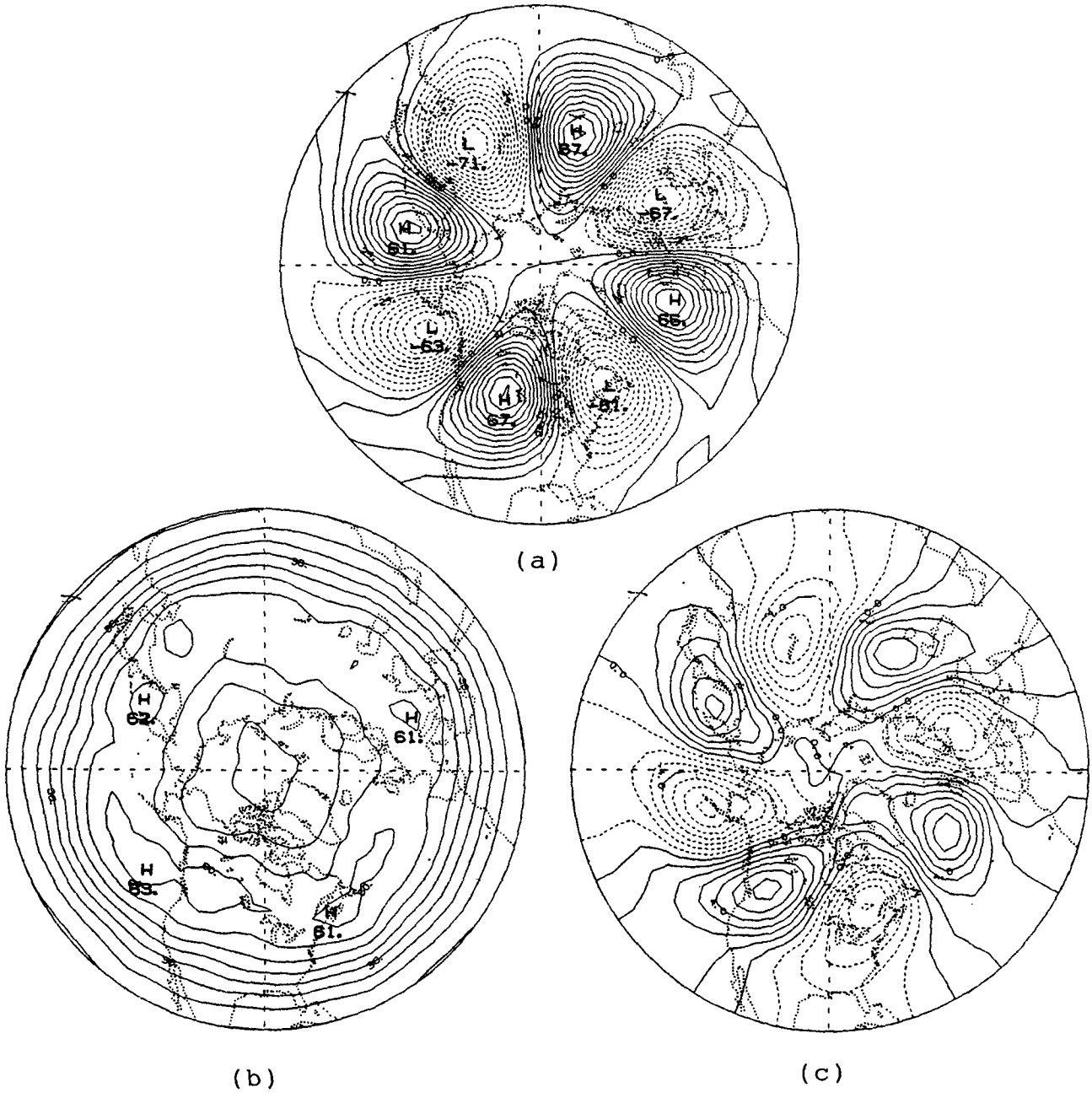

FIG. 8. As in Fig. 5 except for the phase-shifted flow with $m_0 = 4$.

frequency eddies act to reinforce the low-frequency wave and to slow down its eastward propagation.

f. Phase-shifted flow relative to the traveling storm tracks

The results reported in sections 5b–5e are obtained by performing the phase shifting transformation following a low-frequency wave of the geopotential height. We have repeated the above calculations with a phase shifting transformation that follows a low-frequency wave in the tendency field induced by the high-frequency eddies. To do so, we need to change the definition λ^* in (5) to

$$\lambda^*(t;\phi_0) = \frac{360}{2\pi}\frac{(\vartheta^L_{m_0}(\phi_0,t) - \vartheta^S_{m_0}(\phi_0) - 2\pi\mathcal{R}_{m_0}(t))}{m_0}, \quad \phi_0 = 50°\text{N}, \tag{8}$$

where, $\vartheta^L_{m_0}(\phi_0, t)$ is the phase angle of the m_0 wave of $\chi^L_h(\lambda, \phi_0, t)$, the low-frequency component of the tendency field induced by the high-frequency eddies. $\vartheta^S_{m_0}(\phi_0)$ is deliberately taken to be the phase angle of the time-mean tendency field shown in panel (c) of Figs. 5–8 so that we may compare the new results to those found in sections 5b–5e. We may interpret the resulting flow as the flow phase-shifted relative to the traveling storm tracks. If the symbiotic relation between low-frequency flow and high-frequency eddies were to hold not only in the statistical sense but equally at each observation time, the phase-shifting transformation (8) would be identical to the phase-shifting transformation (5).

Here we only present a representative case of such a phase-shifted flow, namely for $m_0 = 4$ (Fig. 9). The

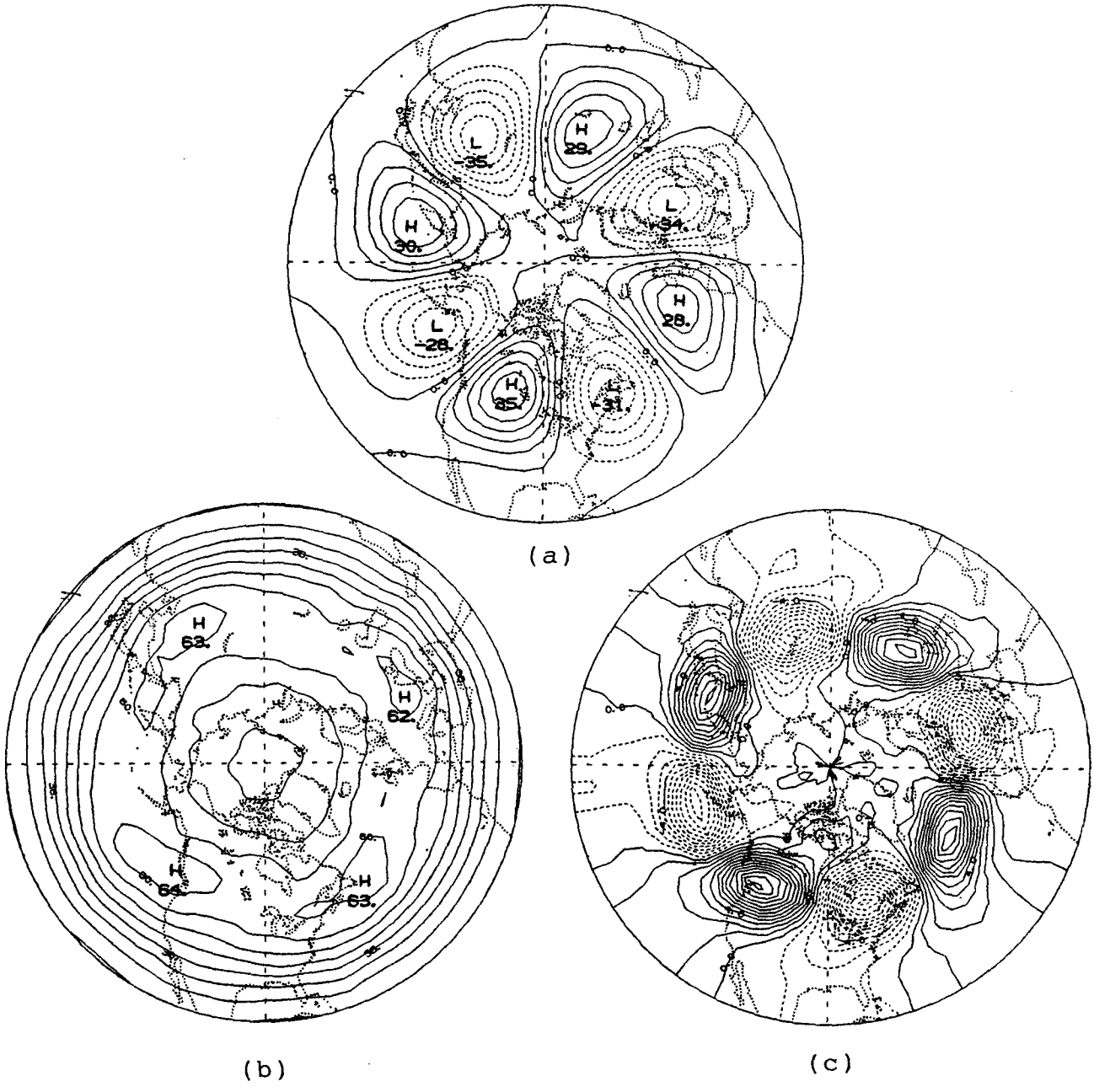

FIG. 9. As in Fig. 5 except for the phase-shifted flow following the low-frequency wavenumber 4 of the instantaneous tendency field induced by the high-frequency eddies.

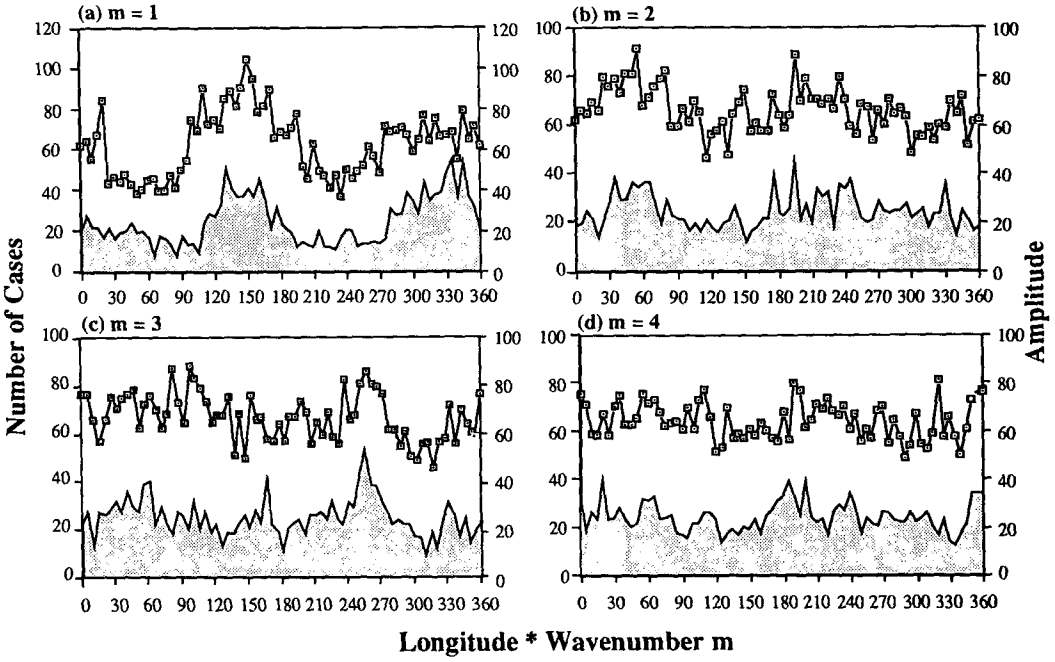

Fig. 10. Histograms of the frequency of occurrence of the first ridge position east of Greenwich of low-frequency wave m_0 at 50°N as a function of longitude boxes (the shaded area). The width of each of the boxes is $5/m_0$ degrees. The curve connecting the squares is the amplitude (in the unit of gpm) of the wave averaged over all the cases of the ridge occurring in the same longitude box. (a) $m_0 = 1$. (b) $m_0 = 2$. (c) $m_0 = 3$. (d) $m_0 = 4$.

same relation between the low-frequency planetary scale wave and its traveling storm tracks identified with (5) and presented in Fig. 8 is now also seen in Fig. 9. Particularly, the phase difference between the traveling wave and the high-frequency forcing field is about the same for the two phase-shifted flows. The intensity of the traveling storm tracks deduced with (8) appear to be stronger. The amplitude of the feedback field is about twice as large as that shown in Fig. 8c whereas the amplitude of the corresponding traveling planetary scale wave is only about half of that shown in Fig. 8a. The difference between Figs. 8 and 9 suggests that the symbiotic relation between low-frequency flow and high-frequency eddies deduced from the statistics of the phase-shifted flows does not hold equally at all times. In the mean the feedback field is neither slower nor faster than the low-frequency waves. But the relative phase does change over time, the forcing and the slowing-down relationship being the most common.

6. Separation of traveling and stationary storm tracks

Obviously, panel (a) of Figs. 5–8 has no signal from the stationary wave since we have removed the stationary waves from the data prior to our analyses. One may question, however, whether the zonal inhomogeneity in panel (b) of these figures could only consist of traveling storm tracks. Unlike the stationary waves, we cannot remove the stationary storm tracks prior to our analyses because the storm tracks are mathematically defined in terms of the time-mean of a second-moment quantity. The purpose of this section is to report the results of a series of experiments using the 10 year winter data, showing empirically that the zonal inhomogeneity on a rms map of the phase-shifted high-frequency eddies (i.e., panel (b) in Figs. 5–8) has little signal from the stationary storm tracks so that we may attribute the zonal inhomogeneity on such a map to the traveling storm tracks.

Intuitively, it is quite reasonable to assume that the zonally inhomogeneous part of the rms field observed in the original coordinate (i.e., Fig. 1b) would become zonally uniform in a moving frame provided that the moving frame does not have too much preference in some particular longitudinal sectors in time. To examine whether the frame moving with a low-frequency wave m_0 has a preference to occur in some longitudinal sectors, we plot in Fig. 10 the histogram of the first ridge position east of Greenwich of a low-frequency wave m_0 at 50°N as a function of longitude boxes from 0° to $360°/m_0$ for $m_0 = 1$, 2, 3, and 4. The width of each of the boxes is $5/m_0$ degrees. Also shown in Fig. 10 is the amplitude of the wave averaged over all the cases when the first ridge hits the longitude box in question. Obviously, the frame moving with low-frequency wave m_0 is not purely uniform in longitude

(otherwise the number of cases in each box would be exactly equal to 25). Particularly, the frame moving along with $m_0 = 1$ has some preference over the longitude sectors where the low-frequency variability is maximum. It is also not surprising to see the frequent occurrence of the higher amplitude of the wavenumber 1 of these two longitude sectors. As m_0 increases, the frequency of occurrence of the ridge east of Greenwich becomes nearly uniform in longitude over the domain of $(0°, 360°/m_0)$. The randomizer $\mathcal{R}_{m_0}(t)$ effectively enlarges the nearly uniform domain to the full range (0°, 360°) by randomly selecting the m_0 possible positions for the low-frequency wave m_0 with an equal possibility. Hence, the moving frame defined in (5) with $m_0 \geq 2$ practically has little preference over any longitudinal sector.

Since our hope on separating the traveling storm tracks from the stationary ones is placed on the phase shifting technique, it is desirable to confirm whether the same technique is capable of separating the traveling from the stationary waves. Applying (5) to the unfiltered wave flow $z^W(\lambda, \phi, t)$ (which includes stationary waves, low-frequency waves, and high-frequency eddies) and constructing the time mean map of the phase-shifted flow thus obtained yields that

$$\overline{\widehat{z^W}(\lambda, \phi, t)} \approx \overline{\widehat{z^{LW}}(\lambda, \phi, t)}$$

(note that $\overline{\widehat{z^{LW}}(\lambda, \phi, t)}$ corresponds to the map shown in panel (a) of Figs. 5–8). This implies that the phase shifting operation relative to a low-frequency wave m_0 ($m_0 = 1, 2, 3,$ and 4) can remove not only the stationary waves but also all other transient waves so that the only survivor on the map $\overline{\widehat{z^W}(\lambda, \phi, t)}$ is the low-frequency wave m_0 itself. Hence the phase shifting technique is as good as a filtering technique in terms of removing the stationary waves from the data. This also suggests that Fig. 10a features a distribution that is sufficiently uniform in longitude for the current purpose.

As discussed in section 4, we have

$$\chi_h(\lambda, \phi, t) \equiv -\nabla^{-2}\left\{\frac{f_0}{g}\nabla\cdot(\hat{\mathbf{v}}^h\hat{\zeta}^h)\right\} = \widehat{\chi_h}(\lambda, \phi, t)$$

$$\equiv -\nabla^{-2}\left\{\frac{f_0}{g}\nabla\cdot(\mathbf{v}^h\zeta^h)\right\}, \qquad (9)$$

where $\chi_h(\lambda, \phi, t)$ is the instantaneous feedback field calculated from the phase-shifted high-frequency eddies and $\widehat{\chi_h}(\lambda, \phi, t)$ is the phase-shifted instantaneous feedback field associated with the (unshifted) high-frequency eddies. Equation (9) enables us to apply (5) directly to $\chi_h(\lambda, \phi, t)$ to recover the maps shown in panel (c) of Figs. 5–8, since

$$\overline{\widehat{\chi_h}(\lambda, \phi, t)} \equiv \overline{\chi_h(\lambda, \phi, t)}.$$

We have particularly applied (5) to $\chi'_h(\lambda, \phi, t)$ field, the transient part of the tendency field induced by the high-frequency eddies ($\chi'_h(\lambda, \phi, t) = \chi_h(\lambda, \phi, t) - \overline{\chi_h(\lambda, \phi, t)}$). Since we have interpreted $\overline{\chi_h(\lambda, \phi, t)}$ as the feedback field of the stationary storm tracks upon the stationary waves, the maps shown in panel (c) of Figs. 5–8 would be completely free from the feedback field of the stationary storm tracks if $\overline{\widehat{\chi'_h}(\lambda, \phi, t)} = \overline{\chi_h(\lambda, \phi, t)}$. The results of this set of experiments indeed show that $\overline{\widehat{\chi'_h}(\lambda, \phi, t)} \approx \overline{\chi_h(\lambda, \phi, t)}$. This finding again strongly suggests that the zonal inhomogeneity in the rms map of the phase-shifted high-frequency eddies [i.e., panel (c) of Figs. 5–8] practically is free from the zonal inhomogeneity shown in Fig. 1b.

7. Conclusions

This paper has documented the existence of the traveling storm tracks and their relation to the low-frequency flow with 10-year winter data of 500 mb geopotential height over the Northern Hemisphere. The symbiotic relation between the low-frequency waves and the traveling storm tracks is found in a coordinate system that moves with the phase speed of an individual low-frequency planetary scale wave. The main conclusions are:

1) The phase-shift technique is capable of separating the traveling from the stationary storm tracks. This technique is useful for studying the time mean structure of the low-frequency wave and their propagation. By following a well-defined structure in the low-frequency field, we can isolate both this structure and the attendant storm tracks.

2) The decrease of the amplitude of the low-frequency waves with the zonal wavenumber is much less dramatic than is the case for the stationary waves. The ratio of the time mean amplitude of a low-frequency wave to that of a stationary wave is 0.7 for $m = 1$, 0.8 for $m = 2$, 1.0 for $m = 3$ and much larger than 1.0 for $m > 3$. The low-frequency waves $m = 1$ ($m = 2$) exhibit a well-defined tripolar (dipolar) pattern in the meridional direction. The low-frequency wavenumber 3 and 4, on the other hand, are dominated with a monopole structure in the meridional direction. In general the meridional scale increases with the zonal wavenumber.

3) Statistically, there exists a traveling storm track downstream of each trough of a traveling planetary scale wave. For $m = 1$ and 2, there are also traveling storm tracks northwest of the ridges. The vorticity flux of the high-frequency eddies associated with the traveling storm tracks tends to reinforce the low-frequency waves and to retard their propagation. The effect of the vorticity flux associated with the high-frequency

eddies on the propagation of the low-frequency waves perhaps explains the large discrepancy between the linear and actual phase speeds of the Rossby waves. The relation between the low-frequency flow and the traveling storm tracks resembles that between the stationary waves and the stationary storm tracks.

Our findings support earlier works indicating that a substantial amount of the low-frequency variability of the midlatitude atmospheric circulation can be explained by the forcing of the high-frequency eddies. These low-frequency waves appear to organize the high-frequency eddies so that the latter preferentially intensify downstream of the troughs of the former.

We have not addressed in this paper why each of the low-frequency planetary scale waves has its own storm tracks. One of the potential mechanisms is the local instability of a single planetary scale wave embedded in the zonal flow. If that is the case, then the intensification of the high-frequency eddies downstream of each trough of a planetary scale wave would have to occur simultaneously. Another potential candidate is the local instability of the (instantaneous) total low-frequency flow embedded in the zonal flow. In this case, the preferential development of the high-frequency eddies would primarily take place downstream of the major troughs that are contributed collectively by all the low-frequency waves. As a result, it would still be possible that there exist statistically a storm track downstream of each trough of an individual low-frequency wave.

Other issues to be addressed later include: (i) Can one identify the life-cycle of a low-frequency event? Nakamura and Wallace (1990) speak about the life-cycle of low-frequency "events," by which they mean the growth, mature, and decaying stages of a blocking at some fixed geographical locations. We could greatly expand that idea by allowing the low-frequency "events" to move. (ii) In our statistics some of the low-frequency anomalies may actually not be traveling, but are stationary oscillations. Is there a need to distinguish traveling and standing low-frequency variations?

Acknowledgments. We are grateful to Dr. Mankin Mak for helpful suggestions and discussions. The review process helped us to improve the manuscript. Thanks also go to Mr. Ping Tian for assistance in the use of the NCAR graphic package on the IBM 4381 at the University of Maryland. This research was supported by NOAA under Grant NA89-AA-H-MC066.

REFERENCES

Cai, M., and M. Mak, 1990a: On the basic dynamics of regional cyclogenesis. *J. Atmos. Sci.*, **47**, 1417–1442.

——, and ——, 1990b: Symbiotic relation between planetary and synoptic scale waves. *J. Atmos. Sci.*, **47**, 2953–2968.

Blackmon, M. L., 1976: A climatological spectral study of the 500 mb geopotential height of the Northern Hemisphere. *J. Atmos. Sci.*, **33**, 1607–1623.

——, J. M. Wallace, N. C. Lau and S. L. Mullen, 1977: An observational study of Northern Hemisphere wintertime circulation. *J. Atmos. Sci.*, **34**, 1040–1053.

Branstator, G., 1990: Low-frequency patterns induced by stationary waves. *J. Atmos. Sci.*, **47**, 629–648.

Colucci, S. J., 1985: Explosive cyclogenesis and large-scale circulation changes: Implications for atmospheric blocking. *J. Atmos. Sci.*, **42**, 2701–2717.

——, 1987: Comparative diagnosis of blocking versus nonblocking planetary-scale circulation changes during synoptic-scale cyclogenesis. *J. Atmos. Sci.*, **44**, 124–139.

Dole, R. M., 1983: Persistent anomalies of extratropical Northern Hemisphere wintertime circulation. *Large-Scale Dynamical Processes in the Atmosphere.* 95–109. B. J. Hoskins and R. P. Pearce, Eds., Academic Press, 397 pp.

——, 1986: The life cycles of persistent anomalies and blocking over the North Pacific. *Adv. Geophys.*, **29**, 31–68.

Egger, J., and H. D. Schilling, 1983: On the theory of the long-term variability of the atmosphere. *J. Atmos. Sci.*, **40**, 1073–1085.

——, and ——, 1984: Stochastic forcing of planetary scale flow. *J. Atmos. Sci.*, **41**, 779–788.

Frederiksen, J. S., 1983: Disturbances and eddy fluxes in Northern Hemisphere flows: Instability of three-dimensional January and July flows. *J. Atmos. Sci.*, **40**, 836–855.

Gall, R., R. Blakeslee and R. C. J. Somerville, 1979: Cyclone-scale forcing of ultralong waves. *J. Atmos. Sci.*, **36**, 1692–1698.

Green, J. S. A., 1977: The weather during July 1976: some dynamical considerations of the drought, *Weather*, **32**, 120–126.

Hendon, H. H., and D. L. Hartmann, 1985: Variability in a nonlinear model of the atmosphere with zonally symmetric forcing. *J. Atmos. Sci.*, **42**, 2783–2797.

Holopainen, E.O., and C. Fortelius, 1987: High-frequency transient eddies and blocking. *J. Atmos. Sci.*, **44**, 1632–1645.

Hoskins, B. J., I. N. James and G. H. White, 1983: The shape, propagation and mean-flow interaction of large-scale weather systems. *J. Atmos. Sci.*, **40**, 1595–1612.

Illari, L., 1984: A diagnostic study of the potential vorticity in a warm blocking anticyclone. *J. Atmos. Sci.*, **41**, 3518–3526.

Kok, C. J., J. D. Opsteegh and H. M. van den Dool, 1987: Linear models: Useful tools to analyze GCM results. *Mon. Wea. Rev.*, **115**, 1996–2008.

Konrad, C. E. II, and S. J. Colucci, 1988: Synoptic climatology of large-scale circulation changes during explosive cyclogenesis. *Mon. Wea. Rev.*, **116**, 1431–1443.

Lau, N. C., 1988: Variability of the observed midlatitude storm tracks in relation to low frequency changes in the circulation pattern. *J. Atmos. Sci.*, **45**, 2718–2743.

——, and E. O. Holopainen, 1984: Transient eddy forcing of the time-mean flow as identified by geopotential tendencies. *J. Atmos. Sci.*, **41**, 313–328.

MacVean, M. K., 1985: Long-wave growth by baroclinic processes. *J. Atmos. Sci.*, **42**, 1089–1101.

Madden, R. A., and P. Speth, 1989: The average behavior of large-scale westward traveling disturbance evident in the Northern Hemisphere geopotential heights. *J. Atmos. Sci.*, **46**, 3225–3239.

Mak, M., 1990: Dynamics of an atmospheric blocking as deduced from its local energetics. *Quart, J. R. Meteor. Soc.* in press.

Metz, W., 1990: Empirical modeling of extra-tropical cyclone vorticity fluxes. *Tellus*, **42A**, 14–27.

——, 1987: Transient eddy forcing of low-frequency atmospheric variability. *J. Atmos. Sci.*, **44**, 2429–2439.

Mullen, S. L., 1987: Transient eddy forcing of blocking flows. *J. Atmos. Sci.*, **44**, 3–22.

Nakamura, H., and J. M. Wallace, 1990: Observed changes in baro-

clinic wave activity during the life cycles of low-frequency circulation anomalies. *J. Atmos. Sci.*, **47**, 1100–1116.

Opsteegh, J. D., and A. D. Vernekar, 1982: A simulation of the January standing wave patter including the effects of transient eddies. *J. Atmos. Sci.*, **39**, 734–743.

Pierrehumbert, R. T., 1984: Local and global baroclinic instability of zonally varying flow. *J. Atmos. Sci.*, **41**, 2141–2162.

Shabbar, A., K. Higuchi, and J. L. Knox, 1990: Regional analysis of Northern Hemisphere 500 kPa geopotential height from 1946 to 1985. *J. Climate*, **3**, 543–557.

Shutts, G. J., 1983: The propagation of eddies in diffluent jetstreams: eddy vorticity forcing of 'blocking' flow fields. *Quart. J. R. Meteor. Soc.*, **109**, 737–761.

Simmons, A. J., J. M. Wallace and G. W. Branstator, 1983: Barotropic wave propagation and instability, and the atmospheric teleconnection patterns. *J. Atmos. Sci.*, **40**, 1363–1392.

Van den Dool, H. M., 1982: What do observations tell about long-range predictability? Koninklijk Nederlands Meteorologisch Instituut workshop: *On the Theory and Application of Simple Climate Models to the Problem of Long Range Weather Prediction.* 1–11. R. Mureau, C. J. Kok, and R. J. Haarsma, Eds., 129 pp.

——, 1989: A new look at weather forecasting through analogues. *Mon. Wea. Rev.*, **117**, 2230–2247.

Wallace, J. M., and M. L. Blackmon, 1983: Observations of low-frequency atmospheric variability. *Large-Scale Dynamical Processes in the Atmosphere.* 55–94. B. J. Hoskins and R. P. Pearce, Eds., Academic Press, 397 pp.